Influence of relative submergence on spatial variance and form-induced stress of gravel-bed flows

James R. Cooper,[1] Jochen Aberle,[2] Katinka Koll,[3] and Simon J. Tait[4]

Received 14 March 2013; revised 5 August 2013; accepted 6 August 2013.

[1] Spatial flow variance has a strong control on sediment transport, sediment-water interface exchange mechanisms, and the distribution and behavior of aquatic organisms in rivers. Thus, being able to quantify spatial flow variance, and how it varies with different water levels, is important for understanding how fluvial processes change during periods of time varying flow. In this paper, laboratory flume measurements of near-bed flow velocity were used to quantify spatial flow variance and form-induced stress, and their variation with flow submergence, within and above the surface of porous, gravel beds with differing grain roughness. The analysis revealed spatial flow variance was usually four or five times higher within the roughness layer than above. A rise in relative submergence resulted typically in a decrease in spatial variance—relative to bed shear velocity—in streamwise form-induced intensity, streamwise turbulence intensity, and form-induced momentum flux, both within and above the roughness layer. Flow submergence had no consistent influence on spatial variance in the vertical flow direction and in Reynolds stress. Form-induced stress was significant within the roughness layer, more so at shallow depths. The greater significance was driven primarily by higher spatial flow variance in time-averaged streamwise velocity at these depths. The implication is the relative role of momentum transfer mechanisms within the roughness layer, and thus, sediment-water interface exchange processes in rivers will change during periods of time varying flows.

Citation: Cooper, J. R., J. Aberle, K. Koll, and S. J. Tait (2013), Influence of relative submergence on spatial variance and form-induced stress of gravel-bed flows, *Water Resour. Res.*, *49*, doi:10.1002/wrcr.20464.

1. Introduction

[2] Spatial flow variance in rivers has a strong control on sediment transport, sediment-water interface exchange mechanisms, and the distribution and behavior of aquatic organisms. For example, spatial flow variance influences the distribution of bed shear stress [e.g., *Bathurst et al*., 1979], promotes the development of in-stream flow refugia [e.g., *Lancaster*, 1999], and affects the spatial pattern of erosion and deposition [e.g., *Konrad et al*., 2002]. Thus, being able to quantify spatial flow variance, and how it varies with different water levels, is important for understanding how fluvial processes change during periods of time varying flow.

[3] A large body of evidence shows that gravel-bed flows are spatially variant. For example, gravel-bed flows comprise turbulent coherent flow structures, such as low-speed wall streaks [e.g., *Grass et al*., 1991], near-wall region bursts (ejections and sweeps) [e.g., *Grass*, 1971], and large-scale flow structures [e.g., *Grass and Mansour-Tehrani*, 1996; *Shvidchenko and Pender*, 2001; *Hardy et al*., 2009] that propagate throughout the depth of the flow. Velocity profiles vary in shape over rough gravel substrates displaying logarithmic, linear, accelerating, and s-shaped profiles [e.g., *Byrd et al*., 2000; *Lawless and Robert*, 2001; *Nikora et al*., 2004; *Lamarre and Roy*, 2005; *Aberle et al*., 2008; *Mignot et al*., 2009a; *Dey and Das*, 2012], revealing variation in the way the flow is organized, both vertically and areally. Others have used double-averaging methodology [see *Nikora et al*., 2007] to quantify the spatial fluctuations in time-averaged velocity, and their contribution to the momentum budget by evaluating form-induced stress [*Aberle et al*., 2008; *Mignot et al*., 2009a, 2009b; *Ferreira et al*., 2010a, 2010b; *Sarkar and Dey*, 2010; *Dey and Das*, 2012]. The focus has been on the influence of bed roughness and geometry on spatial flow structure and form-induced stress. However, there is evidence, albeit piecemeal, that flow submergence also has an important control.

[4] For example, flow measurements both in the laboratory and in the field show that the size of large-scale flow structures change with flow depth. The flow structures have a length of typically three to five flow depths and have a

Additional supporting information may be found in the online version of this article.

[1]Department of Geography and Planning, School of Environmental Sciences, University of Liverpool, Liverpool, UK.
[2]Department of Hydraulic and Environmental Engineering, Norwegian University of Science and Technology, Trondheim, Norway.
[3]Leichtweiss-Institute for Hydraulic Engineering and Water Resources, Technische Universität Braunschweig, Braunschweig, Germany.
[4]School of Engineering, Design and Technology, University of Bradford, Bradford, UK.

Corresponding author: J. R. Cooper, Department of Geography and Planning, School of Environmental Sciences, University of Liverpool, Liverpool, L69 3BX, UK. (james.cooper@liverpool.ac.uk)

0043-1397/13/10.1002/wrcr.20464

width and height that is approximately equal to the flow depth [*Shvidchenko and Pender*, 2001; *Roy et al*., 2004]. In the field, *Lamarre and Roy* [2005] and *Legleiter et al*. [2007] observed that spatial flow organization was controlled by flow depth and not by channel topography.

[5] *Koll* [2006] showed that the shapes of velocity profiles within the logarithmic layer are dependent upon relative submergence (ratio of flow depth to roughness length scale). First, the zero-plane displacement height decreased with increasing submergence. Second, the von Kármán constant increased with a rise in submergence due to the influence of submergence on the scaling of coherent turbulent flow structures, and thus on the gradient of the velocity profile.

[6] A small number of studies have examined the change in spatial variance in time-averaged streamwise velocity with submergence, but the results are inconsistent. The studies have observed an increase in variance with a rise in flow depth [*Clifford*, 1996; *Cooper*, 2012], a decrease [*Buffin-Bélanger et al*., 2006], and little or no change above [*Legleiter et al*., 2007] and within the roughness layer [*Aberle et al*., 2008]. *Aberle et al*. [2008] further showed that relative submergence had little influence on the magnitude of form-induced stress. *Buffin-Bélanger et al*. [2006] explored the variance in other flow properties, observing a decrease in the spatial variance in time-averaged vertical and lateral velocity, and a decrease in the spatial variance in turbulence intensity and turbulent kinetic energy, with an increase in flow depth. However, in the flume experiments conducted by *Buffin-Bélanger et al*. [2006] the water depth decreased with an increase in discharge. Hence, the flow conditions did not reflect how water levels vary in rivers.

[7] In short, there is evidence that flow submergence has an important control on the spatial structure and organization of gravel-bed flows, but the effect of submergence on spatial flow variance is unclear. To date, there has been no systematic study of the effects of submergence on the spatial variance of all the key properties of turbulent flows. A number of important questions remain unanswered for gravel-bed flows. (i) Previous studies have examined the change in spatial variance of time-averaged flow parameters over a single bed and/or over a small range of submergences. Thus, how does spatial variance and form-induced stress change across a broader range of submergences, and are the changes the same for different levels of grain roughness? (ii) Does submergence only affect spatial variance above the roughness layer where the effects of bed geometry are weaker? (iii) How does the spatial variance in vertical velocity compare to the spatial variance in streamwise velocity? (iv) Is the spatial variance in turbulence intensity greater than in time-averaged velocity, and how does the spatial variance in turbulence intensity change with submergence? The paper attempts to answer these questions by combining flow velocity data from experiments conducted by *Aberle et al*. [2008] and *Cooper and Tait* [2010]. These experiments provide spatially distributed velocity measurements of the near-bed flow field over a number of water-worked gravel beds with differing grain roughness, and over a range of different flow submergences. Combining the data from these experiments provides a detailed study on the influence of submergence on the spatial heterogeneity of key near-bed flow parameters.

Table 1. A Summary of the Experimental Conditions[a]

Run	S	Q (m^3/s)	h (m)	h/k
1A	0.0027	0.060	0.130	5.8
2A	0.0027	0.092	0.162	7.3
3A	0.0027	0.116	0.186	8.3
1B	0.0027	0.060	0.141	4.9
2B	0.0027	0.091	0.174	6.0
3B	0.0027	0.121	0.205	7.1
4B	0.0027	0.150	0.229	7.9
5B	0.0027	0.181	0.253	8.8
1C	0.0027	0.061	0.150	3.6
2C	0.0027	0.090	0.184	4.5
3C	0.0027	0.122	0.214	5.2
4C	0.0027	0.150	0.240	5.8
5C	0.0027	0.180	0.261	6.4
6C	0.0027	0.220	0.289	7.0
1D	0.0027	0.061	0.162	2.9
2D	0.0027	0.090	0.196	3.5
3D	0.0027	0.121	0.226	4.1
4D	0.0027	0.150	0.252	4.6
5D	0.0027	0.181	0.275	5.0
6D	0.0027	0.221	0.302	5.5
7D	0.0027	0.251	0.325	5.9
1E	0.0010	0.061	0.193	4.1
2E	0.0010	0.090	0.235	5.0
3E	0.0010	0.121	0.277	5.9
1F	0.0100	0.091	0.171	2.9
2F	0.0100	0.121	0.191	3.2
3F	0.0100	0.181	0.222	3.7
1G	0.0029	0.002	0.023	2.4
2G	0.0029	0.004	0.037	3.7
3G	0.0029	0.006	0.048	4.8
4G	0.0029	0.009	0.060	6.0
5G	0.0029	0.014	0.079	8.0
6G	0.0029	0.028	0.113	11.5
1H	0.0028	0.001	0.024	3.0
2H	0.0028	0.003	0.037	4.7
3H	0.0028	0.005	0.048	6.0
4H	0.0028	0.008	0.059	7.5
5H	0.0028	0.013	0.077	9.7
6H	0.0028	0.025	0.111	14.0

[a] S is the bed slope, Q is the flow discharge, h is the flow depth, and k is the geometric roughness height (range of bed surface elevations $z_{99} - z_{01}$). The letters after the run number denote the studied bed (see Table 2).

2. Methodology

2.1. Data

[8] The *Aberle et al*. [2008] experiments were conducted in a 20 m long and 0.90 m wide tilting flume (runs A–F in Table 1). Two different coarse sediment mixtures (I and II) with 0.63 mm $< D <$ 64 mm (Figure 1a) were used for the development of water-worked gravel surfaces. At the beginning of an experiment, the well-mixed sediment was placed in the flume, and the surface was allowed to armor for a constant discharge (Q_a) until the sediment transport rate became negligible, and a stable armored bed surface was formed. Velocity measurements were made for the bed forming water discharge (Q_a) and for lower discharges ($Q < Q_a$) with a laser Doppler anemometer (LDA; see below). After the velocity measurements had been completed, the bed forming discharge was increased, so that the existing armor layer was destroyed and a new layer

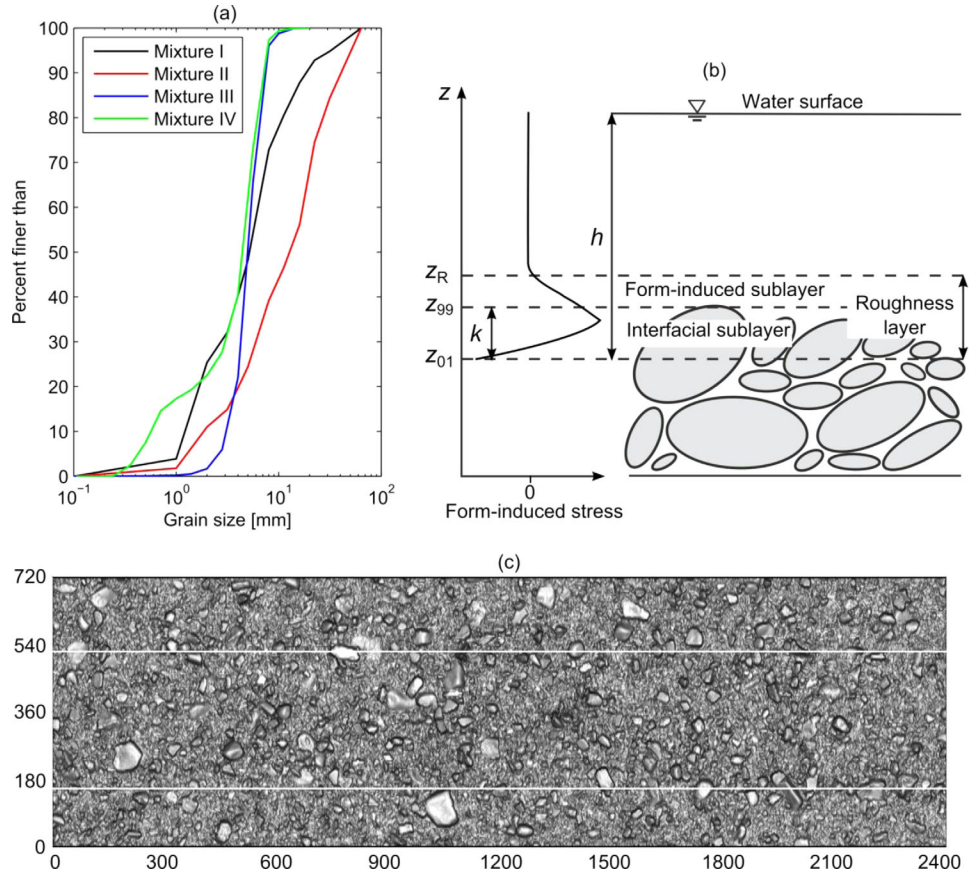

Figure 1. (a) Grain-size distribution of bed mixtures, (b) definition of flow layers and height and distance parameters, and (c) an example DEM of a studied bed surface (bed B). In the DEM the flow direction is from left to right, axis units are in millimeters, and the white lines show the boundaries of the central measurement area of the LDA measurements.

developed. The above velocity measurements were repeated and the procedure continued as long as the bed could stabilize itself without a considerable loss of slope or erosion of the sediment to the flume bottom. Table 2 shows the key grain size and surface topography statistics of the studied armor layers. In the present paper, 27 different flow conditions were used for six different bed surfaces.

[9] For each studied flow, 24–48 randomly distributed vertical profiles of 3-D velocities were measured using a LDA system consisting of a 2-D and a 1-D probe. The measurements were carried out within a 2.4 m long and 0.36 m wide test section, located 9 m downstream of the flume inlet (see Figure 1c). Immersed LDA probes enabled flow velocity measurements within and above the roughness elements. The sampling time at each point was 60 s, and sampling frequencies ranged from ~20 to 100 Hz. The vertical sampling resolution of the velocity measurements was $\Delta z = 2$ mm below roughness tops, $\Delta z = 4$ mm above roughness tops, and $\Delta z = 10$ mm in the outer flow field. The vertical velocity was resolved from the transformation of measured velocities in a probe oriented coordinate system into an orthogonal coordinate system. Measurements were carried out in planes parallel to the bed surface to simplify the spatial averaging procedure.

[10] The *Cooper and Tait* [2010] experiments were conducted in a tilting, 18.3 m long, 0.5 m wide laboratory flume (experiments G–H in Table 1). Two different sediment mixtures were used: a log-normal, unimodal grain-size distribution (III) and a slightly bimodal grain-size distribution (IV). Both had a grain-size range of 0.15 mm $< D <$ 14 mm (Figure 1a) and the bimodal mixture was created by adding 25% sand to the unimodal mixture. Two sediment beds—each using one of the mixtures—were formed by feeding material into running water, with the feed rate twice the estimated flow transport capacity. In each case a deposit formed progressively over time. The

Table 2. A Summary of the Grain Size and Surface Topography Statistics of the Two Beds[a]

Bed	Mixture	Q_a (m^3/s)	D_{50} (m)	D_{84} (m)	k (m)	σ_b (m)
A	I	0.120	0.0111	0.0272	0.0223	0.0048
B	I	0.180	0.0136	0.0287	0.0289	0.0063
C	I	0.220	0.0184	0.0444	0.0410	0.0082
D	I	0.250	0.0196	0.0484	0.0553	0.0108
E	II	0.120	0.0235	0.0440	0.0472	0.0099
F	II	0.180	0.0250	0.0488	0.0594	0.0126
G	III	0.030	0.0050	0.0070	0.0099	0.0021
H	IV	0.030	0.0042	0.0066	0.0080	0.0017

[a] Q_a is the bed forming flow discharge; D_{50} and D_{84} are the grain sizes at which 50% and 84% of the bed material is finer, respectively; k is the range ($z_{99} - z_{01}$); and σ_b is the standard deviation in bed surface elevations.

surfaces were water-worked and armored (see Table 2 for surface topography statistics). Once each bed was formed the bed slope was dropped so the bed shear stress was below the one that formed the deposit, and velocity measurements were made in six runs with different flow discharges (Table 1). Further detailed information on the bed surface topographies, the acquisition of the digital elevation models (DEMs), and how the beds were formed can be found in *Aberle and Nikora* [2006] and *Cooper and Tait* [2009].

[11] Velocities were measured using a 2-D PIV (Particle Image Velocimetry) system, 9.1 m from the flume inlet. PIV measurements were taken in a vertical plane at nine lateral positions across the bed: −88, −66, −44, −22, 0, 22, 44, 66, and 88 mm (a lateral position of 0 mm denotes the centerline of the flume). At each lateral position a streamwise length of 143 mm was imaged, and the flow sampled for 330 s at a sampling frequency of 9 Hz. Streamwise and vertical velocities were measured within and above the roughness elements, at different streamwise and vertical positions. The image analysis provided a maximum of 61 velocity measurements in the streamwise direction at each lateral position. Above the roughness elements, the maximum number of measurements available for spatial averaging was therefore 549 (61 × 9) at a given measurement height. The separation distance between measurements, in both the streamwise and vertical direction, was 2.25 mm.

[12] In both series of tests, the flows were steady, uniform, and fully turbulent and were below those required for bed movement. For the following analysis the vertical coordinate has the origin at z_{01}, and the roughness crest of the bed is taken to be z_{99} (Figure 1b), where z_{xx} is the level at which xx% of observed bed elevations are smaller. These levels were resolved from the detrended laser scans of each of the bed surfaces. The use of these two definitions, rather than z_0 and z_{100}, minimizes the influence of topography measurement errors and local effects due to the random nature of the bed [*Aberle et al*., 2008]. As a consequence, the bed geometric roughness height $k = z_{99} - z_{01}$. Moreover, the detrended laser scans of the beds were used to determine the standard deviation of bed elevations σ_b (see Table 2).

[13] The different flow layers within the roughness layer are defined based on *Nikora et al*. [2001]. The interfacial sublayer occupies the flow region between roughness crest and trough, and the form-induced sublayer is the flow region that exists above the interfacial sublayer and is composed entirely of fluid (Figure 1b). This sublayer is termed "form-induced" to reflect the appearance of form-induced stress due to flow separation from the roughness elements below. Together the two layers make up the roughness layer; the upper boundary of the form-induced sublayer is the upper boundary of the roughness layer.

2.2. Temporal and Spatial Averaging

[14] For each experiment, the collected velocity data were used to derive turbulence and spatial flow characteristics in the streamwise and vertical directions. First, the instantaneous velocity data were time-averaged (denoted by a straight overbar), and a Reynolds decomposition was applied. Then, the time-averaged data were decomposed into spatially averaged (denoted by angle brackets) and spatially fluctuating (denoted by a wavy overbar) components, such that $\overline{u}_i = \langle \overline{u}_i \rangle + \tilde{u}_i$, where u_i is the instantaneous velocity in the ith direction [e.g., *Nikora et al*., 2007]. This technique is known as double averaging (temporal and spatial averaging). The spatial fluctuations arise from the difference between the double-averaged $\langle \overline{u}_i \rangle$ and time-averaged $\overline{u}_i$ values, similar to the conventional Reynolds decomposition of $u'_i = u_i - \overline{u}_i$, where u'_i is the temporal fluctuation. Almost all previous studies (see above) that have used double averaging have focused on presenting double-averaged flow parameters (e.g., double-averaged velocity and spatially averaged Reynolds stress) to gain insight into the average behavior of the flow over the entire bed. The interest of the current paper is not in this average behavior but in how the flow behavior varies over the bed, and the impact this variation has on momentum transfer between the flow and a porous, gravel bed.

[15] The analysis quantifies spatial flow variance and its contribution to momentum transfer by examining the following: (i) form-induced intensities $\sqrt{\langle \tilde{u}^2 \rangle}$ and $\sqrt{\langle \tilde{w}^2 \rangle}$ which are the standard deviation in $\overline{u}$ and $\overline{w}$, and a measure of the spatial flow variance in time-averaged streamwise and vertical velocities, respectively; (ii) spatial variance in turbulence intensities $\sqrt{\overline{u'^2}}$ and $\sqrt{\overline{w'^2}}$, quantified by the standard deviation (over space) in $\sqrt{\overline{u'^2}}$ and $\sqrt{\overline{w'^2}}$, denoted by σ_{Tu} and σ_{Tw}, respectively; (iii) spatial variance in Reynolds stress $\overline{u'w'}$, quantified by the standard deviation (over space) in $\overline{u'w'}$ (denoted by σ_R); (iv) form-induced stress $\langle \tilde{u}\tilde{w} \rangle$; and (v) spatial variance in form-induced momentum flux $\tilde{u}\tilde{w}$, quantified by the standard deviation in $\tilde{u}\tilde{w}$ (denoted by σ_F).

[16] The terms above are not often explored; so some further description is necessary. The form-induced intensities measure the variation in the time-averaged behavior of the flow over the bed. Flow parameters σ_{Tu} and σ_{Tw} are measures of the spatial variance in turbulent behavior over the bed, and σ_R is a measure of the spatial variance in fluid shear stress due to turbulent activity. Given that Reynolds stress at a single location depends on the magnitude of turbulent velocity fluctuations and their cross product, σ_R is due to spatial variance in turbulent velocity fluctuations and temporal coherency (e.g., bursting activity) over the bed. The form-induced stress is the streamwise-averaged momentum flux that arises due to spatial variance in the time-averaged flow. Because form-induced stress is given by spatially averaging the point-to-point spatial fluctuations in time-averaged velocity, its magnitude depends on both the magnitude of spatial variance in the time-averaged flow and on the spatial coherency (or structuring) of the time-averaged flow. Thus, form-induced stress is a result of "persistent structures" in the time-averaged flow, such as persistent vortices behind roughness elements, or vortices shed from large roughness elements. The parameter σ_F is a measure of the spatial variance in momentum flux caused by these persistent structures. The analysis will explore the vertical profiles of each of the flow measures, and their change with relative submergence (those profiles not presented in the manuscript can be found online in the supporting information section).

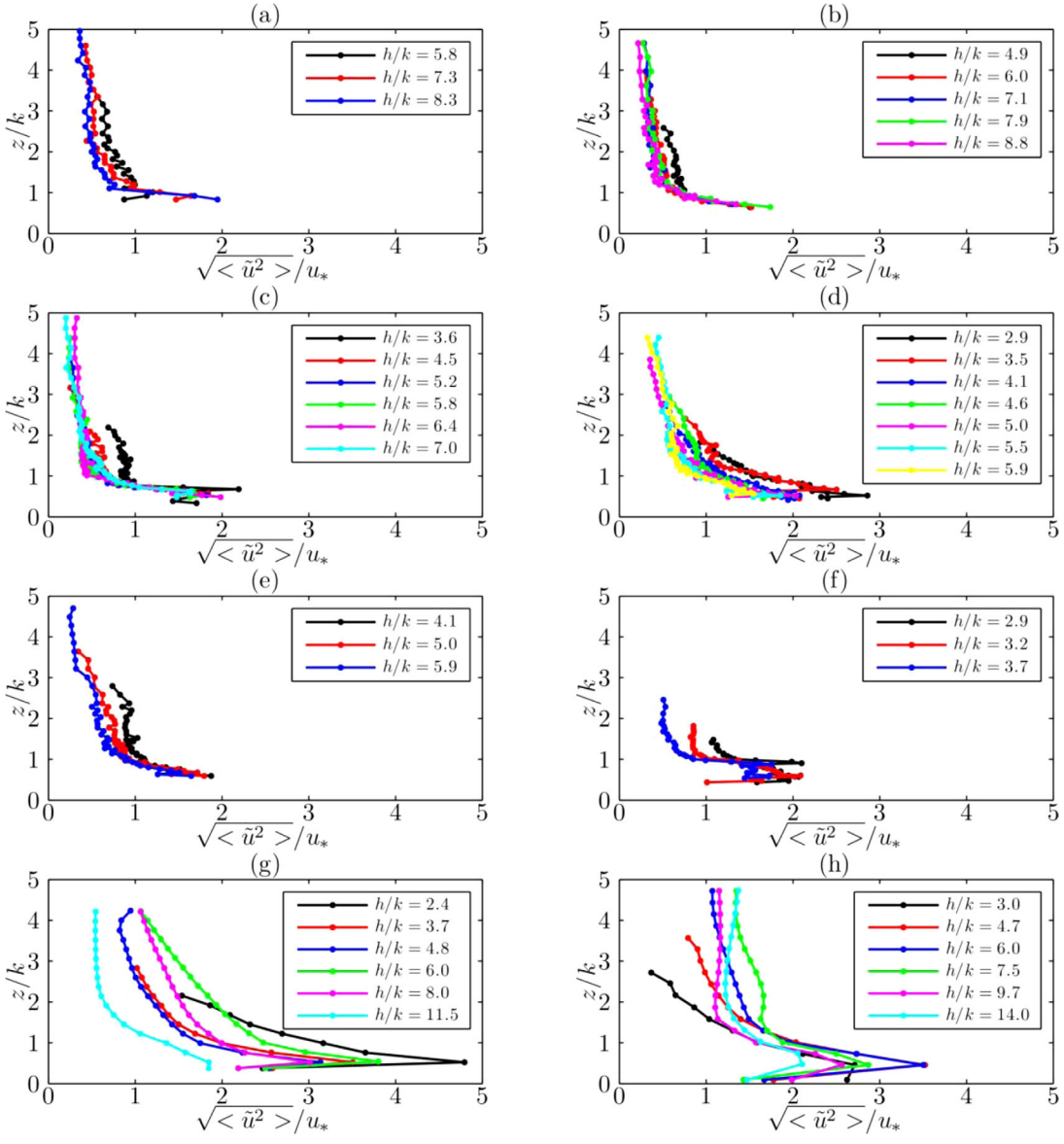

Figure 2. Vertical profiles of streamwise form-induced intensity at different levels of relative submergence for beds (a) A, (b) B, (c) C, (d) D, (e) E, (f) F, (g) G, and (h) H.

[17] Previous studies examined changes in absolute values of spatial flow variance with submergence, and the results were inconsistent. In this study, the shear velocity is used to scale the above measures of spatial flow variance for two reasons: first, to allow direct comparison of the flow data in *Aberle et al*. [2008] and *Cooper and Tait* [2010] and second, to determine whether a consistent trend emerges when differences in flow conditions are accounted for by using scaled measures of spatial flow variance. The shear velocity is defined by $u_* = \sqrt{\tau_0/\rho}$ where τ_0 is the total fluid stress at the roughness crest; a definition argued by *Manes et al*. [2007] to be most suitable for scaling flows of differing submergence. The total fluid stress was estimated by linearly extrapolating the spatially averaged Reynolds stress from the layer above the bed surface down to z_{99}. The relative height above the minimum bed elevation z_{01} is defined as z/k.

3. Results

3.1. Form-Induced Intensity

[18] The vertical profiles of the relative streamwise form-induced intensity $\sqrt{\langle \tilde{u}^2 \rangle}/u_*$ reveal four main observations (Figure 2). First, all profiles exhibit the same general shape. Spatial flow variance attains a maximum value within the upper half of the interfacial sublayer and declines with distance away from the roughness crest up to a height of $\sim$1–2k above the roughness crest, above which the variance is fairly constant. Below the peak value in the interfacial sublayer the variance typically reduces toward the roughness trough and remains higher than above the bed. Second, the spatial flow variance is not negligible above the bed. Between the roughness crest and a height of $\sim$1–2k above the roughness crest, the spatial variance is

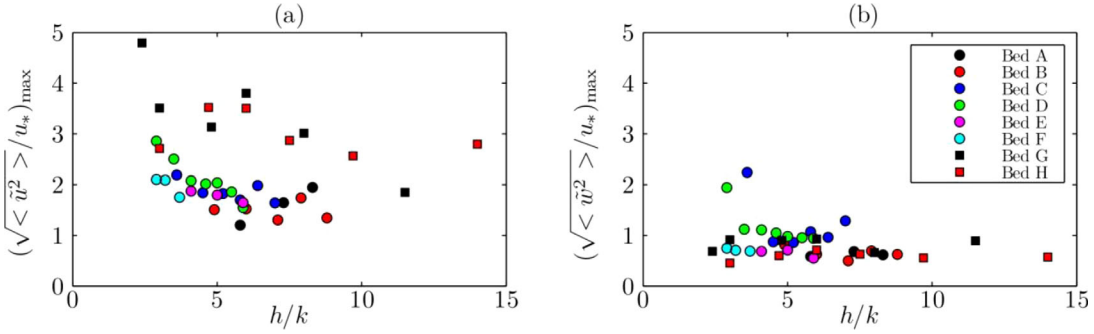

Figure 3. Change in (a) maximum streamwise form-induced intensity and (b) maximum vertical form-induced intensity with relative submergence. For clarity the legend is only shown in Figure 3b and is the same for Figure 3a.

half of the peak magnitude within the interfacial sublayer, regardless of the bed roughness or flow submergence. Third, for tests with comparable flow submergence, $\sqrt{\langle\tilde{u}^2\rangle}/u_*$ is higher for beds G and H (Figures 2 and 3a; discussed below). Finally, relative submergence has a strong influence on the magnitude of $\sqrt{\langle\tilde{u}^2\rangle}/u_*$. At a given measurement height the streamwise form-induced intensity is typically higher at the lower submergences, even within the interfacial sublayer. The rate of change in intensity with submergence is similar for all the beds (Figure 3a).

[19] The results for vertical form-induced intensity $\sqrt{\langle\tilde{w}^2\rangle}/u_*$ are different: there is a negligible difference in intensity for flows of differing submergence (Figure 3b). The profiles of $\sqrt{\langle\tilde{w}^2\rangle}/u_*$ (Figure S1 in supporting information) have a similar shape to those of $\sqrt{\langle\tilde{u}^2\rangle}/u_*$, and the spatial variance in $\overline{w}$ is around half the variance in $\overline{u}$.

3.2. Spatial Variance in Turbulence Intensity

[20] The spatial variance in streamwise turbulence intensity σ_{Tu}, like the streamwise form-induced intensity, reduces with a rise in submergence, and at a similar rate for different levels of grain roughness (Figure 4a and Figure S2 in supporting information). The spatial variance in streamwise turbulence intensity is typically half the variance in $\overline{u}$.

[21] The spatial variance in vertical turbulence intensity σ_{Tw} changes little with submergence (Figure 4b and Figure S3 in supporting information). The spatial variance in vertical turbulence intensity is ~50% lower than in streamwise turbulence intensity, and similar to the variance in $\overline{w}$.

3.3. Spatial Variance in Reynolds Stress

[22] The spatial variance in Reynolds stress is large in relation to the spatially averaged Reynolds stress at the roughness crest (Figure 5); in the flow above the bed the variance is ~10–50%, and up to nearly three times higher in the interfacial sublayer. For tests with comparable flow submergence, spatial variance in Reynolds stress is consistently higher for beds G and H (discussed below). Variance in Reynolds stress is of a similar magnitude to the variance in streamwise turbulence intensity, and around half the spatial variance in $\overline{u}$. The profiles reveal no consistent dependency between spatial variance in Reynolds stress and flow submergence.

3.4. Form-Induced Stress

[23] At distances ~$1-2k$ above the roughness crest, form-induced stress is negligible (Figure 6). Between this distance and the roughness crest, form-induced stress begins to become more significant, up to 20% of the spatially averaged Reynolds stress at the roughness crest. Form-induced stress continues to increase within the interfacial sublayer, often reaching a first peak, and then either decreasing or switching from making a negative to a positive contribution

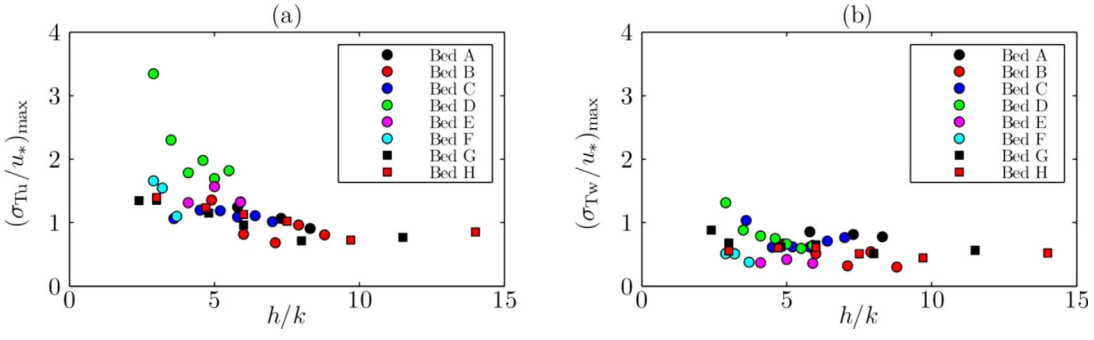

Figure 4. Change in (a) maximum standard deviation in streamwise turbulence intensity and (b) maximum standard deviation in vertical turbulence intensity.

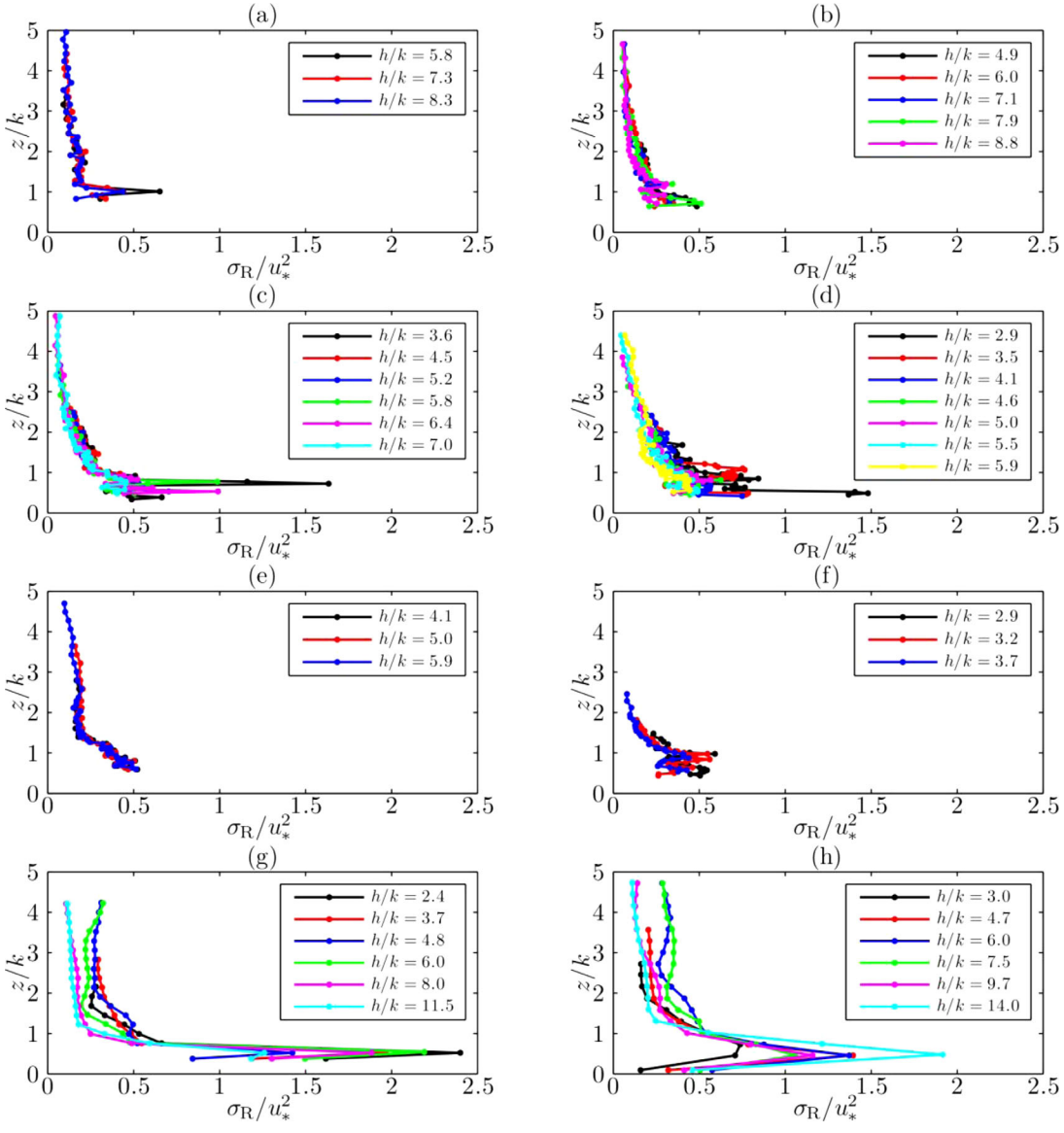

Figure 5. Vertical profiles of standard deviation in Reynolds stress at different levels of relative submergence for beds (a) A, (b) B, (c) C, (d) D, (e) E, (f) F, (g) G, and (h) H.

to fluid stress. This switch and the existence of peaks within the roughness elements is due to the dependence of form-induced stress on the sign of $\tilde{u}$ and $\tilde{w}$, and hence on the manner in which the time-averaged flow is coherently structured. In these experiments a positive value of $-\langle\tilde{u}\tilde{w}\rangle/u_*^2$ defines a situation in which the spatial coherence in the time-averaged flow field extracts momentum from the flow in the streamwise direction. A negative value defines a situation in which form-induced stress enhances the fluid momentum in the streamwise direction. Within the interfacial sublayer, form-induced stress is much larger, typically up to ±20–50% of the Reynolds stress at the roughness crest and in some cases, is close to being equal to the Reynolds stress at the crest. Form-induced stress typically—but not consistently—makes a greater contribution to shear stress (positive or negative) at the lower submergences, coinciding well with the observed increase in the streamwise form-induced intensities with a decrease in submergence.

3.5. Spatial Variance in Form-Induced Momentum Flux

[24] Profiles of spatial variance in form-induced momentum flux (Figure 7) display a similar shape to those seen earlier, except the values are much smaller at large distances above the interfacial sublayer because form-induced stress is very low. Within the interfacial sublayer, the variance in form-induced momentum flux is typically a decade higher than form-induced stress indicating that form-induced flux is highly variant spatially, more so at the lower submergences. For the majority of tests, the spatial variance in form-induced momentum flux within the interfacial sublayer is of a similar magnitude to the variance in Reynolds stress. Given that form-induced stress is always lower than Reynolds stress, the similarity reveals much greater spatial variation in form-induced momentum flux around its spatial mean than in Reynolds stress.

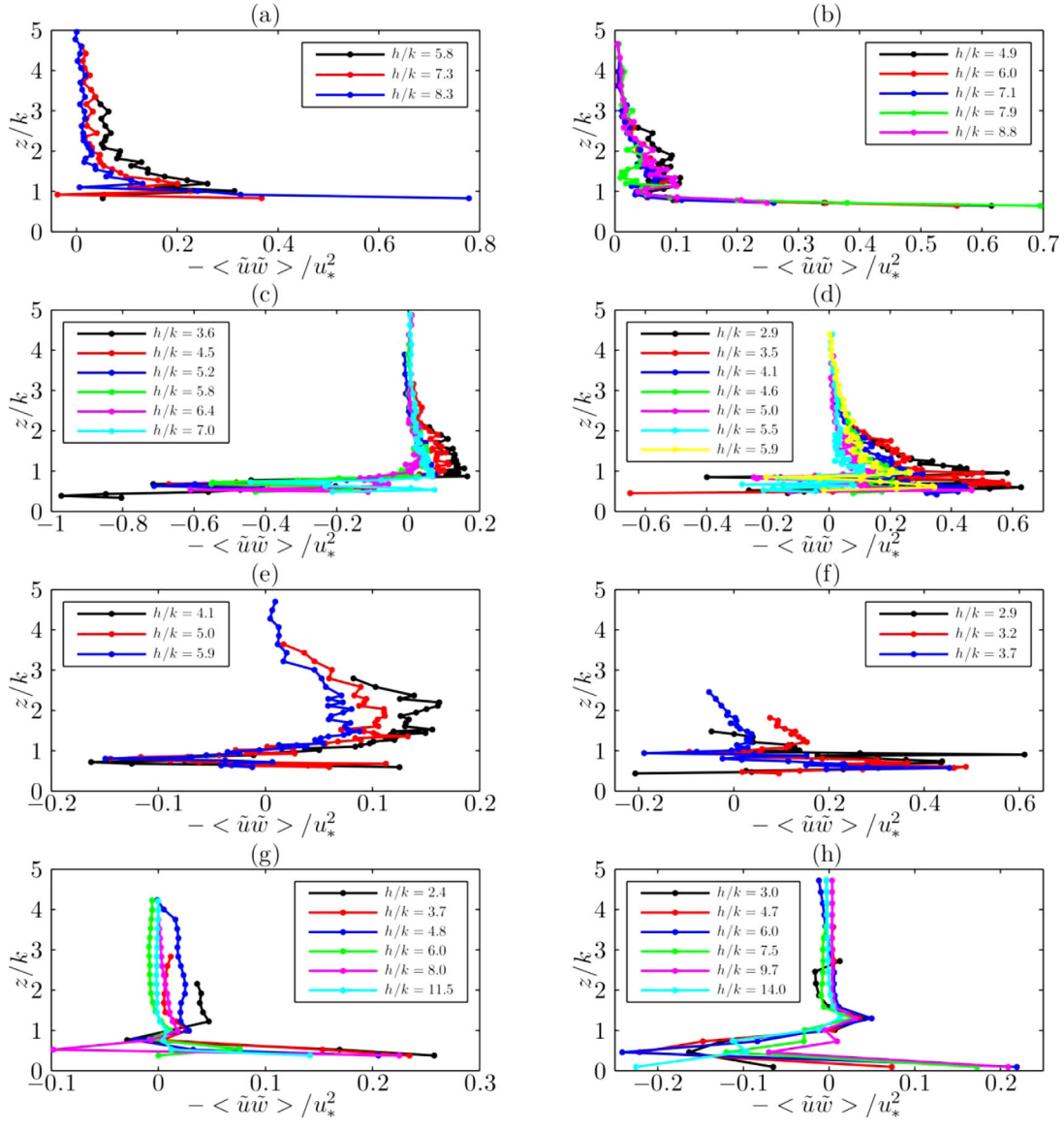

Figure 6. Vertical profiles of form-induced stress at different levels of relative submergence for beds (a) A, (b) B, (c) C, (d) D, (e) E, (f) F, (g) G, and (h) H. Note the different scales on the horizontal axis due to the variation in sign of form-induced stress.

4. Discussion

4.1. Influence of Relative Submergence on Spatial Flow Variance

[25] A rise in relative submergence resulted typically in a decrease in the relative spatial flow variance in streamwise form-induced intensity, streamwise turbulence intensity, and form-induced momentum flux, both within and above the roughness layer. Flow submergence had no consistent or appreciable influence on spatial variance in the vertical flow direction and in Reynolds stress. These results were consistent for beds of differing levels of grain roughness. A key result is that normalized spatial variance, at a given height, changed with submergence within the interfacial sublayer and at low, "roughness dominated," submergences, conditions in which the magnitude of spatial flow variance was previously assumed strongly (or entirely) controlled by bed geometry.

[26] The changes in variance in the streamwise flow direction reflect the scaling of coherent flow structures with flow depth [*Shvidchenko and Pender*, 2001; *Roy et al.*, 2004; *Lamarre and Roy*, 2005]: at lower depths, over a given measurement area, more structures are likely to be present at any one time than at higher depths, resulting in a more spatially complex flow. For static beds, where bursting consistently occurs at the same location, the scaling with depth will affect the variance in time-averaged as well as instantaneous flow, as reflected in the scaling of longitudinal time-averaged flow structures with depth [*Cooper and Tait*, 2008]. Given the spatial variance in Reynolds stress is a product of the variation in temporal flow coherency over the bed, a consistency in the location of bursting activity could also offer a possible explanation for why the spatial variance in Reynolds stress did not change consistently with submergence. The observation that changes in variance with submergence only occur in the streamwise direction might be

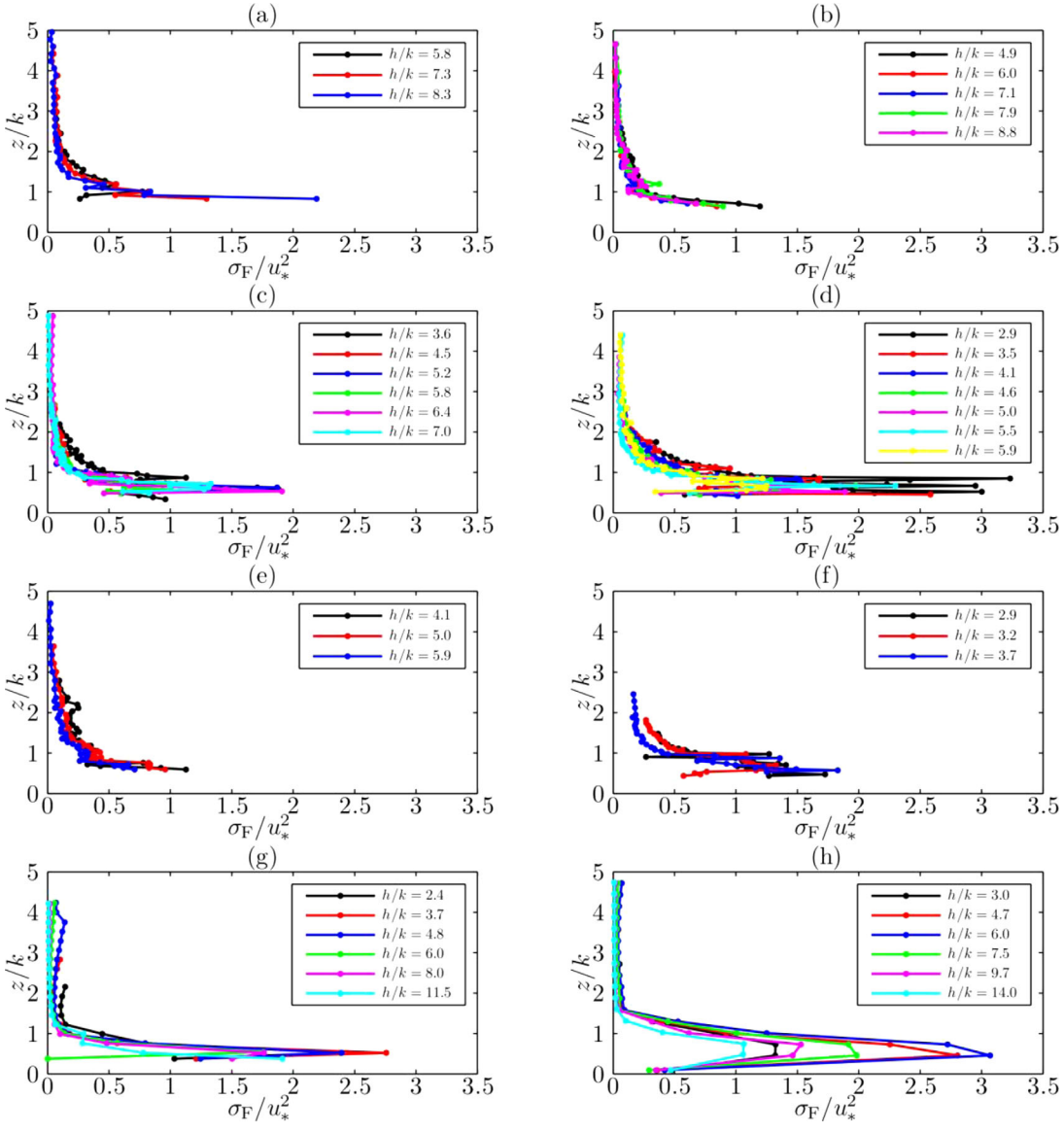

Figure 7. Vertical profiles of standard deviation in form-induced momentum flux at different levels of relative submergence for beds (a) A, (b) B, (c) C, (d) D, (e) E, (f) F, (g) G, and (h) H.

because the streamwise length of large-scale flow structures vary more greatly with depth than their vertical dimension [*Shvidchenko and Pender*, 2001; *Roy et al*., 2004].

[27] Previous studies examined changes in absolute values of spatial flow variance with submergence, and the results were inconsistent. When the differences in flow conditions were accounted for by using scaled measures of spatial flow variance, a general trend emerged for particular flow properties, thus going some way to explaining the discrepancy in previous work. However, when the flow data of *Buffin-Bélanger et al*. [2006] are scaled, the reverse is found. This contradiction can be resolved by considering the flow conditions studied by *Buffin-Bélanger et al*. [2006]. In their experiments, the water depth decreased with an increase in discharge. Hence, the spatial heterogeneity, as interpreted by *Buffin-Bélanger et al*. [2006], is strongly influenced by flow nonuniformity.

[28] The present paper has examined beds with different levels of grain roughness. It might be assumed that the strong effects of relative submergence are restricted to these particular conditions and when larger scales of roughness are present, like form roughness, the effect would be significantly diminished. However, three pieces of evidence question this assumption. First, the changes in spatial flow variance with relative submergence also occur where form roughness is present [*Clifford*, 1996]. Second, the spatial organization of the flow field is dependent on flow depth at different scales: the grain scale [*Shvidchenko and Pender*, 2001; *Cooper and Tait*, 2008; *Hardy et al*., 2009], patch scale [*Roy et al*., 2004; *Buffin-Bélanger et al*., 2006], and reach scale [*Clifford*, 1996; *Lamarre and Roy*, 2005; *Legleiter et al*., 2007]. For example, at the reach scale, *Legleiter et al*. [2007] demonstrated that an increase in flow stage resulted in the spatial structure of time-averaged velocity becoming "smoother and more continuous" [*Legleiter et al*., 2007, p. 343], as the more localized influence of bed surface topography became increasingly drowned out, resulting in flow depth being the primary

Table 3. A Comparison of Spatial Flow Variance and Form-Induced Stress Data From Previous Studies[a]

Study	Bed Properties	$\sqrt{\langle\tilde{u}^2\rangle}/u_*$	$\sqrt{\langle\tilde{w}^2\rangle}/u_*$	$-\langle\tilde{u}\tilde{w}\rangle/u_*^2$	h/k
Present paper[b]	A: water-worked, unimodal gravel, $D_{50} = 11$ mm	0.2–2.0	0.1–0.7	−0.1–0.8	5.8–8.3
	B: water-worked, unimodal gravel, $D_{50} = 14$ mm	0.3–1.8	0.1–0.8	0–0.7	4.9–8.8
	C: water-worked, unimodal gravel, $D_{50} = 18$ mm	0.3–2.2	0.1–2.3	−1.0–0.2	3.6–7.0
	D: water-worked, unimodal gravel, $D_{50} = 20$ mm	0.4–2.8	0.1–1.9	−0.7–0.6	2.9–5.9
	E: water-worked, unimodal gravel, $D_{50} = 24$ mm	0.4–1.9	0.1–0.7	−0.7–0.2	4.1–5.9
	F: water-worked, unimodal gravel, $D_{50} = 25$ mm	0.5–2.1	0.4–0.8	−0.2–0.6	2.9–3.7
	G: water-worked, unimodal gravel, $D_{50} = 5.0$ mm	0.5–4.8	0.2–0.9	−0.1–0.3	2.4–11.5
	H: water-worked, bimodal gravel sand, $D_{50} = 4.4$ mm	0.4–3.5	0.2–0.7	−0.3–0.2	3.0–14.0
Buffin-Bélanger et al. [2006][b]	Cast of water-worked bed, $D_{50} = 17$ mm	0.7–2.8[c]			5.4–7.8
Legleiter et al. [2007][d]	Cobble-bed riffle, $D_{50} = 124$ mm	1.2–1.3	0.18–0.2		0.5–0.7[e]
Mignot et al. [2009a][b]	Random[f], unimodal gravel, $D_{50} = 20$ mm			−0.01–0.08	3.5
Mignot et al. [2009b][b]	Random[f], unimodal gravel, $D_{50} = 20$ mm			−0.05–0.1[g]	3.5
Ferreira et al. [2010a][b]	Random[f], varying proportions of sand, gravel $D_{50} = 28$ mm	0.2–4.6		−0.7–0.4	3.0
		0.2–3.5		−0.5–0.2	3.1
		0.2–5.9		−0.7–0	3.3
		0.2–7.0		−0.05–1.1	3.0
				−0.1–0.4	5.1
Franca et al. [2010][d]	Gravel armor layer, $D_{50} = 68$ mm	0.2–2.8	0–0.1		2.9
Sarkar and Dey [2010][b]	Random[f], uniform gravel, $D_{50} = 25$ mm			0–0.1	5.6
Dey and Das [2012][b]	Random[f], uniform gravel, $D_{50} = 40$ mm	0–0.8	0–0.2	0–0.2	12.2

[a]Note that there are no data from previous studies on spatial variance in turbulent flow parameters.
[b]Laboratory study.
[c]Predicted using regression models and measurement heights presented in *Buffin-Bélanger et al*. (2006).
[d]Field study.
[e]k is predicted by D_{95}.
[f]Gravel was not water-worked but placed within the flume.
[g]Values are for different areas of the bed.

control on the reach-scale structuring of the flow. *Lamarre and Roy* [2005] showed the flow field was dominated by coherent patterns associated with reach-scale variations in depth rather than by abrupt, isolated changes associated with bed topography. Thus, the evidence in *Lamarre and Roy* [2005] and *Legleiter et al*. [2007] counters the intuitive assumption that the effect of flow depth will be significantly diminished when larger scales of roughness, such as form roughness, are present. Third, the changes in spatial variance correlate with the scaling of turbulent flow structures with flow depth observed for various scales of bed roughness [*Shvidchenko and Pender*, 2001; *Roy et al*., 2004; *Lamarre and Roy*, 2005]. It is interesting to note that the strong control of submergence on flow properties has also been observed for bed surfaces composed of regular patterns of fixed roughness shapes (e.g., spheres) [*Manes et al*., 2007] and also smooth beds [*Nakagawa and Nezu*, 1981; *Imamoto and Ishigaki*, 1986; *Komori et al*., 1989; *Liu et al*., 2001]. Work is required to test the evidence further and compare changes in spatial flow variance with submergence for different scales of bed roughness.

4.2. Vertical Distribution of Spatial Flow Variance and Form-Induced Stress

[29] The normalized spatial flow variance at a given height changed with relative submergence, but the vertical distribution (profile shape) within the interfacial sublayer was found to vary little for a particular bed surface. In particular, the peak in flow spatial variance and the smaller spikes in the profiles, for a particular bed, were nearly always located at the same height within the interfacial sublayer. Also, the spatial flow variance became small and reasonably constant at the same height of ∼1 to 2k above the roughness crest. The consistency in profile shape for different flows over the same bed suggests that bed geometry has a strong control on the vertical distribution of flow variance, and relative submergence does not.

[30] The profile shapes, for a given bed, were also consistent for form-induced stress. Form-induced stress became negligible at a height of ∼1 to 2k above the roughness crest, a height that coincides with the distance that spatial flow variance became small. The height of 1–2k above the roughness crest reflects the height at which persistent vortices behind roughness elements extend above the roughness crest, and provides an estimate of the height of the roughness layer and the upper boundary of the form-induced sublayer. The height is similar to previous observations [*Ferreira et al*., 2010b; *Sarkar and Dey*, 2010]. The consistency in the height of the form-induced sublayer reveals the roughness layer thickness to be invariant with relative submergence, as shown by *Koll* [2006].

[31] Form-induced stress is dependent on the sign and product of $\tilde{u}$ and $\tilde{w}$. Thus, the consistency in profile shapes of form-induced stress for differing flow conditions, and the difference in sign between the different bed surfaces, suggests that roughness geometry has a strong control on the presence of persistent flow structures within the time-averaged flow of the interfacial sublayer.

4.3. Comparison of Levels of Spatial Flow Variance for Various Bed Surfaces

[32] Table 3 shows a comparison of spatial flow variance and form-induced stress data for the different gravel beds, including those of previous studies. As well as allowing a direct comparison between different studies, the data in Table 3 highlight current limitations in understanding of the spatial properties of the near-bed flow field. Table 3 reveals five key observations. First, spatial flow variance and form-induced stress vary between the studies but fall within a

similar, broad range, remarkable given the differences in the studied conditions. The reasons for the differences between the studies are unclear. For the present study, apart from the streamwise form-induced intensities and the spatial variance in Reynolds stress, the difference in values between the beds was partly attributable to differences in submergence because variance changed at a similar rate with submergence. For example, the range of submergences in the tests by *Cooper and Tait* [2010] was greater than those by *Aberle et al*. [2008] so changes were more noticeable in the former. Differences between the data of the two studies [*Aberle et al*., 2008; *Cooper and Tait*, 2010] could also be attributed to differences in the number and arrangement of the velocity measurements; the regular grid of PIV measurements is more likely to detect systematic changes in the organization of the flow with submergence than the randomly located LDA measurements. Thus, differences in velocity sampling as well as relative submergence could contribute to the variation in values between all the studies in Table 3. However it is unclear how differences in bed topography influence the variation for three reasons: (i) in the present study, when differences in spatial flow variance and form-induced stress were analyzed against different roughness properties (e.g., standard deviation in bed elevation, geometric roughness height, and grain-size percentiles) no systematic change was found; (ii) *Dey and Das* [2012], in comparing their form-induced stress values to those measured by *Mignot et al*. [2009a] and *Sarkar and Dey* [2010], showed that form-induced stress increases with roughness size. However, there was an order-of-magnitude difference in submergence between the three studies so a direct comparison was not possible; and (iii) *Ferreira et al*. [2010a], for tests at comparable submergences, revealed form-induced intensities varied little with bed roughness.

[33] The second key observation from Table 3 is that form-induced stress makes both a positive and negative contribution to the momentum budget. *Aberle et al*. [2008] showed the sign of $-\tilde{u}\tilde{w}$ varied with measurement location and therefore with topography, and *McLean and Nikora* [2006] found $\tilde{w}$ usually attains positive values above the upstream slope of a cobble. Why form-induced stress makes a positive contribution to the momentum budget in some studies, but a negative in others, and how the specific properties of the interfacial sublayer cause this difference in sign, remains unclear.

[34] Third, Table 3 reveals that only two field studies [*Legleiter et al*., 2007; *Franca et al*., 2010] have quantified spatial flow variance. Based on the small number of comparisons in Table 3, the normalized spatial flow variance in the laboratory is comparable to the variance in a river, but whether the measures of variance are scalable is unknown.

[35] Fourth, no other study has quantified the spatial flow variance in turbulent activity in the same way as the present study. The values remain peculiar to the gravel surfaces used here until comparisons with other gravel beds are made.

[36] Finally, the profiles of spatial flow variance presented within the studies in Table 3 all display the same general shape: high spatial flow variance within the interfacial sublayer, often displaying spikes, and a quick reduction toward the roughness crest, and above the roughness layer the values are low. Why spikes appear is unclear. The spikes are seemingly unrelated to the roughness geometry function ("porosity" of the interfacial layer) because porosity changes smoothly with depth [e.g., *Aberle*, 2007]. *Aberle et al*. [2008] suggested the spikes occur because of the presence of large roughness elements within the layer that make a large contribution to the total level of spatial flow variance and form-induced stress.

4.4. Implications for Measuring Bed Shear Stress

[37] The presence of form-induced stress and spatial variance in Reynolds stress has a number of implications for measuring bed shear stress. First, the shear stress experienced by some parts of the bed will be different from others. Thus, the shear stress acting upon the boundary cannot be estimated using single-point velocity measurements, regardless of whether the stress is estimated through the extrapolation of a velocity profile or the measurement of Reynolds stress. Spatially distributed velocity measurements are required to account for spatial variance in velocity and Reynolds stress. Secondly, form-induced stress must be quantified [*Manes et al*., 2007; *Nikora et al*., 2007]. Third, form-induced stress is lower than Reynolds stress at a given height indicating a greater spatial variation in form-induced momentum flux around its spatial mean than in Reynolds stress. Thus, to obtain a spatially representative estimate of form-induced stress is more difficult than gaining an estimate of spatially averaged Reynolds stress. Fourth, an accurate estimate of form-induced stress is likely to be more difficult for shallow flows due to the larger variance in form-induced momentum flux. Finally, Reynolds stress makes a larger contribution to the momentum budget so an accurate estimate of the budget hinges more on an accurate estimate of Reynolds stress than of form-induced stress. An accurate estimate of spatially averaged Reynolds stress is more difficult within the interfacial sublayer because, although the stress is lower, spatial variance in Reynolds stress is higher so the variance becomes more pronounced relative to the spatial mean.

4.5. Why Is Form-Induced Stress More Significant for Shallow Flows?

[38] Form-induced stress, relative to Reynolds stress at the roughness crest, was larger in shallow flows, indicating that the relative role of momentum transfer mechanisms, and thus sediment-water interface exchange processes, will change with flow submergence during periods of time varying flows in a river.

[39] Why is form-induced stress more significant for shallow flows? Form-induced stress arises from the correlations between point-to-point spatial deviations in time-averaged velocity. It therefore depends on both the spatial coherence and magnitude of spatial variance in the time-averaged flow. The shape of the form-induced stress and spatial flow variance profiles were similar within the interfacial sublayer. Therefore, the greater significance at shallow depths is unlikely to be due to changes in the spatial coherency or an adjustment of the flow around the roughness elements. Instead, the greater significance is most likely due to higher spatial flow variance, relative to the shear velocity, within the time-averaged flow at these depths. This argument is in agreement with theoretical analysis by *Giménez-Curto and Corniero Lera* [1996] for

oscillatory flows. In addition, spatial variance in time-averaged streamwise velocity was higher than in time-averaged vertical velocity. Thus, the larger form-induced stress at shallow depths is predominately due to larger variance in time-averaged streamwise velocity.

5. Conclusions

[40] The paper describes the results from two sets of laboratory flume experiments, in which spatially distributed velocity measurements were made of the near-bed flow field over water-worked gravel beds with differing grain roughness. Combining the data from these experiments provided a detailed study on the influence of submergence on the spatial heterogeneity of key near-bed flow parameters. The tests sought to quantify spatial flow variance and form-induced stress within and above the surface of porous, gravel beds, and their variation with relative submergence. The main results and inferences can be summarized as follows:

[41] Spatial flow variance was typically four or five times higher within the roughness layer than above and was small and reasonably invariant with distance above a height of one to two vertical roughness lengths above the roughness crest.

[42] A rise in relative submergence resulted typically in a decrease in spatial variance—relative to bed shear velocity—in streamwise form-induced intensity, streamwise turbulence intensity, and form-induced momentum flux, both within and above the roughness layer. Flow submergence had no consistent or appreciable influence on spatial variance in the vertical flow direction and in Reynolds stress.

[43] Spatial variance in turbulent flow parameters (turbulence intensity and Reynolds stress) was of a similar magnitude to the variance in the time-averaged flow, and variance in the vertical flow direction was considerably lower than in the streamwise flow direction.

[44] Form-induced stress was significant up to a height of one to two vertical roughness lengths above the roughness crest. This height revealed the roughness layer thickness to be invariant with relative submergence, coinciding well with previous observations.

[45] The profile shape of spatial flow variance and form-induced stress varied little for a given bed surface suggesting bed geometry had a strong control on the vertical distribution of spatial flow variance and the vertical organization of the time-averaged flow within the roughness layer. Relative submergence had little influence.

[46] Form-induced stress was more significant at shallow depths. The greater significance was primarily driven by higher spatial flow variance in time-averaged streamwise velocity at these depths. The implication is the relative role of momentum transfer mechanisms within the roughness layer, and thus, sediment-water interface exchange processes will change in rivers during periods of time varying flows.

[47] **Acknowledgments.** The LDA data were acquired with support of DFG (Deutsche Forschungsgemeinschaft; contract DI-651/4-3). The comments of the editorial team, Francesco Comiti, and three anonymous reviewers have acted to strengthen the paper and are gratefully acknowledged.

References

Aberle, J. (2007), Measurements of armour layer roughness geometry function and porosity, *Acta Geophys.*, *55*(1), 23–32, doi:10.2478/s11600-006-0036-5.

Aberle, J., and V. Nikora (2006), Statistical properties of armored gravel bed surfaces, *Water Resour. Res.*, *42*, W11414, doi:10.1029/2005WR004674.

Aberle, J., K. Koll, and A. Dittrich (2008), Form induced stresses over rough gravel-beds, *Acta Geophys.*, *56*(3), 584–600, doi:10.2478/s11600-008-0018-x.

Bathurst, J. C., C. R. Thorne, and R. D. Hey (1979), Secondary flow and shear stress at river bends, *J. Hydraul. Div. Am. Soc. Civ. Eng.*, *105*(10), 1277–1295.

Buffin-Bélanger, T., S. Rice, I. Reid, and J. Lancaster (2006), Spatial heterogeneity of near-bed hydraulics above a patch of river gravel, *Water Resour. Res.*, *42*, W04413, doi:10.1029/2005WR004070.

Byrd, T. C., D. J. Furbish, and J. Warburton (2000), Estimating depth-averaged velocities in rough channels, *Earth Surf. Processes Landforms*, *25*(2), 167–173, doi:10.1002/(SICI)1096–9837(200002)25:2<167::AID-ESP66>3.0.CO;2-G.

Clifford, N. J. (1996), Morphology and stage-dependent flow structure in a gravel-bed river, in Coherent Flow Structures in Open Channels, edited by P. J. Ashworth et al., pp. 545–566, John Wiley, Chichester, U. K.

Cooper, J. R. (2012), Does flow variance affect bedload flux when the bed is dominated by grain roughness?, *Geomorphology*, *141*, 160–169, doi:10.1016/j.geomorph.2011.12.039.

Cooper, J. R., and S. J. Tait (2008), The spatial organisation of time-averaged streamwise velocity and its correlation with the surface topography of water-worked gravel beds, *Acta Geophys.*, *56*(3), 614–641, doi:10.2478/s11600-008-0023-0.

Cooper, J. R., and S. J. Tait (2009), Water-worked gravel beds in laboratory flumes—A natural analogue?, *Earth Surf. Processes Landforms*, *34*(3), 384–397, doi:10.1002/esp.1743.

Cooper, J. R., and S. J. Tait (2010), Spatially representative velocity measurement over water-worked gravel beds, *Water Resour. Res.*, *46*, W11559, doi:10.1029/2009WR008465.

Dey, S., and R. Das (2012), Gravel-bed hydrodynamics: Double-averaging approach, *J. Hydraul. Eng.*, *138*(8), 707–725, doi:10.1061/(ASCE)HY.1943–7900.0000554.

Ferreira, R. M. L., M. Amatruda, J. Simão, A. M. Ricardo, M. J. Franca, and C. Di Cristo (2010a), Influence of bed morphology on double-averaged turbulent quantities in low submergence gravel-bed flows, in *River Flow 2010*, edited by A. Dittrich et al., pp. 67–74, Bundesanst. für Wasserbau, Braunschweig, Germany.

Ferreira, R. M. L., L. M. Ferreira, A. M. Ricardo, and M. J. Franca (2010b), Impacts of sand transport on flow variables and dissolved oxygen in gravel-bed streams suitable for salmonid spawning, *River Res. Appl.*, *26*(4), 414–438, doi:10.1002/rra.1307.

Franca, M. J., R. M. L. Ferreira, A. H. Cardoso, and U. Lemmin (2010), Double-average methodology applied to turbulent gravel-bed river flows, in *River Flow 2010*, edited by A. Dittrich et al., pp. 59–65, Bundesanst. für Wasserbau, Braunschweig, Germany.

Giménez-Curto, L. A., and M. A. C. Corniero Lera (1996), Oscillating turbulent flow over very rough surfaces, *J. Geophys. Res.*, *101*(C9), 20,745–20,758, doi:10.1029/96JC01824.

Grass, A. J. (1971), Structural features of turbulent flow over smooth and rough boundaries, *J. Fluid. Mech.*, *50*(2), 233–255, doi:10.1017/S0022112071002556.

Grass, A. J., and M. Mansour-Tehrani (1996), Generalized scaling of coherent bursting structures in the near-wall region of turbulent flow over smooth and rough boundaries, in *Coherent Flow Structures in Open Channels*, edited by P. J. Ashworth et al., pp. 40–61, John Wiley, Chichester, U. K.

Grass, A. J., R. J. Stuart, and M. Mansour-Tehrani (1991), Vortical structures and coherent motion in turbulent-flow over smooth and rough boundaries, *Philos. Trans. R. Soc. London A*, *336*(1640), 35–65.

Hardy, R. J., J. L. Best, S. N. Lane, and P. E. Carbonneau (2009), Coherent flow structures in a depth-limited flow over a gravel surface: The role of near-bed turbulence and influence of Reynolds number, *J. Geophys. Res.*, *114*, F01003, doi:10.1029/2007JF000970.

Imamoto, H., and T. Ishigaki (1986), Visualization of longitudinal eddies in an open channel flow, in *Proceedings of the Fourth International Symposium on Flow Visualization, Flow Visualization IV*, edited by C. Veret, pp. 333–337, Hemisphere, Washington, D. C.

Koll, K. (2006), Parameterisation of the vertical velocity profile in the wall region over rough surfaces, in *Proceedings of the International Conference on Fluvial Hydraulics, River Flow 2006*, edited by R. M. L. Ferreira et al., pp. 163–171, Taylor and Francis, London.

Komori, S., Y. Murakami, and H. Ueda (1989), The relationship between surface-renewal and bursting motions in an open-channel flow, *J. Fluid. Mech.*, *203*, 103–123, doi:10.1017/S0022112089001394.

Konrad, C. P., D. B. Booth, S. J. Burges, and D. R. Montgomery (2002), Partial entrainment of gravel bars during floods, *Water Resour. Res.*, *38*(7), 1104, doi:10.1029/2001WR000828.

Lamarre, H., and A. G. Roy (2005), Reach scale variability of turbulent flow characteristics in a gravel-bed river, *Geomorphology*, *68*(1–2), 95–113, doi:10.1016/j.geomorph.2004.09.033.

Lancaster, J. (1999), Small-scale movements of lotic macroinvertebrates with variations in flow, *Freshwater Biol.*, *41*(3), 605–619, doi:10.1046/j.1365–2427.1999.00410.x.

Lawless, M., and A. Robert (2001), Scales of boundary resistance in coarse-grained channels: Turbulent velocity profiles and implications, *Geomorphology*, *39*(3–4), 221–238, doi:10.1016/S0169–555X(01)00029-0.

Legleiter, C. J., T. L. Phelps, and E. E. Wohl (2007), Geostatistical analysis of the effects of stage and roughness on reach-scale spatial patterns of velocity and turbulence intensity, *Geomorphology*, *83*(3–4), 322–345, doi:10.1016/j.geomorph.2006.02.022.

Liu, Z., R. J. Adrian, and T. J. Hanratty (2001), Large-scale modes of turbulent channel flow: Transport and structure, *J. Fluid. Mech.*, *448*, 53–80, doi:10.1017/S0022112001005808.

Manes, C., D. Pokrajac, and I. McEwan (2007), Double-averaged open-channel flows with small relative submergence, *J. Hydraul. Eng.*, *133*(8), 896–904, doi:10.1061/(ASCE)0733–9429(2007)133:8(896).

McLean, S. R., and V. I. Nikora (2006), Characteristics of turbulent unidirectional flow over rough beds: Double-averaging perspective with particular focus on sand dunes and gravel beds, *Water Resour. Res.*, *42*, W10409, doi:10.1029/2005WR004708.

Mignot, E., E. Barthelemy, and D. Hurther (2009a), Double-averaging analysis and local flow characterization of near-bed turbulence in gravel-bed channel flows, *J. Fluid. Mech.*, *618*, 279–303, doi:10.1017/S0022112008004643.

Mignot, E., D. Hurther, and E. Barthelemy (2009b), On the structure of shear stress and turbulent kinetic energy flux across the roughness layer of a gravel-bed channel flow, *J. Fluid. Mech.*, *638*, 423–452, doi:10.1017/S0022112009990772.

Nakagawa, H., and I. Nezu (1981), Structure of space-time correlations of bursting phenomena in an open-channel flow, *J. Fluid. Mech.*, *104*, 1–43, doi:10.1017/S0022112081002796.

Nikora, V., D. Goring, I. McEwan, and G. Griffiths (2001), Spatially averaged open-channel flow over rough bed, *J. Hydraul. Eng.*, *127*(2), 123–133, doi:10.1061/(ASCE)0733–9429(2001)127:2(123).

Nikora, V., K. Koll, I. McEwan, S. McLean, and A. Dittrich (2004), Velocity distribution in the roughness layer of rough-bed flows, *J. Hydraul. Eng.*, *130*(10), 1036–1042, doi:10.1061/(ASCE)0733-9429(2004)130:10(1036).

Nikora, V., I. McEwan, S. McLean, S. Coleman, D. Pokrajac, and R. Walters (2007), Double-averaging concept for rough-bed open-channel and overland flows: Theoretical background, *J. Hydraul. Eng.*, *133*(8), 873–883, doi:10.1061/(ASCE)0733–9429(2007)133:8(873).

Roy, A. G., T. Buffin-Bélanger, H. Lamarre, and A. D. Kirkbride (2004), Size, shape and dynamics of large-scale turbulent flow structures in a gravel-bed river, *J. Fluid. Mech., 500*, 1–27, doi:10.1017/S0022112003006396.

Sarkar, S., and S. Dey (2010), Double-averaging turbulence characteristics in flows over a gravel bed, *J. Hydraul. Res.*, *48*(6), 801–809, doi:10.1080/00221686.2010.526764.

Shvidchenko, A. B., and G. Pender (2001), Macroturbulent structure of open-channel flow over gravel beds, *Water Resour. Res.*, *37*(3), 709–719, doi:10.1029/2000WR900280.